Dynamics of intrathermocline vortices in a gyre flow over a seamount chain

Mikhail A. Sokolovskiy, Boris N. Filyushkin & Xavier J. Carton

Ocean Dynamics
Theoretical, Computational and Observational Oceanography

ISSN 1616-7341
Volume 63
Number 7

Ocean Dynamics (2013) 63:741-760
DOI 10.1007/s10236-013-0628-y

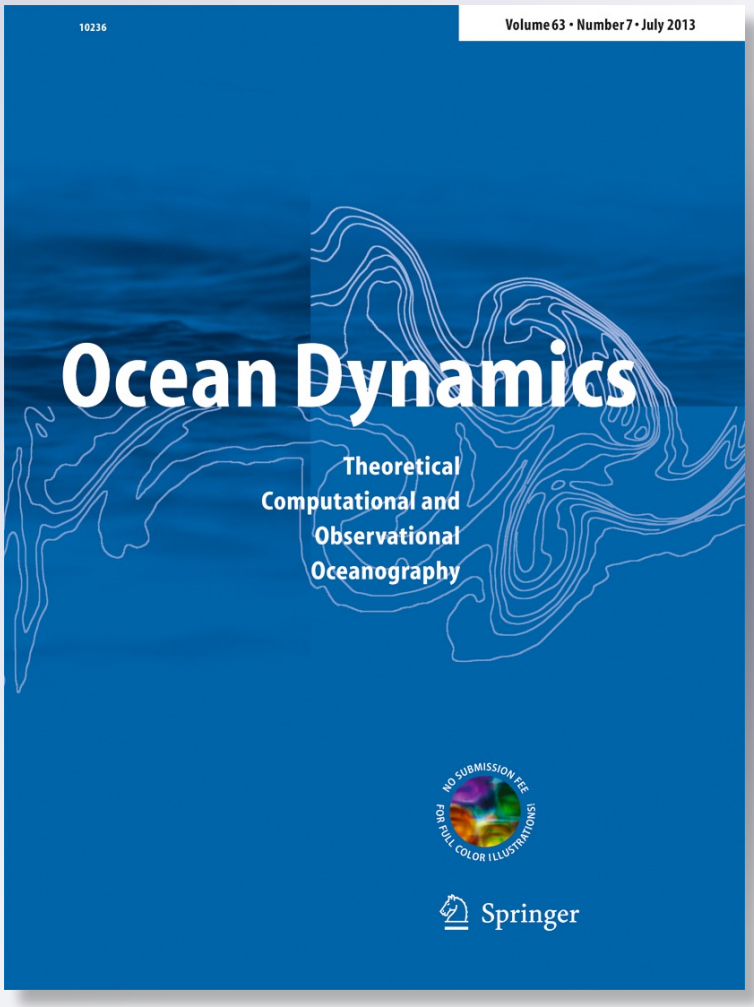

Springer

Ocean Dynamics (2013) 63:741–760
DOI 10.1007/s10236-013-0628-y

Dynamics of intrathermocline vortices in a gyre flow over a seamount chain

Mikhail A. Sokolovskiy · Boris N. Filyushkin · Xavier J. Carton

Received: 15 August 2012 / Accepted: 21 May 2013 / Published online: 14 June 2013

Abstract The interaction of meddies with a complex distribution of seamounts is studied in a three-layer quasi-geostrophic model on the *f*-plane. This study aims at understanding if and how this seamount chain can represent a barrier to the propagation of these eddies and how it can be involved in their decay. The eddies are idealized as vortex patches in the middle layer, interacting with a regional cyclonic current and with ten idealized seamounts. The numerical code is based on the contour surgery technique. The initial position, radius, shape, number and polarity of the eddies are varied. The main results are the following: (1) Though they do not describe the unsteady flow, the streamlines of the regional and topographic flow provide a useful estimate of the vortex trajectories, in particular towards the major seamounts, where stronger velocity shears are expected. (2) The tallest and widest seamounts which have the largest vorticity reservoir are able to considerably erode the vortices, but also to draw anticyclones towards the seamount top. The ability of narrower seamounts to erode vortices is related to their multiplicity. (3) Only 1/3 of the anticyclones with about 30-km radius reach the southern boundary of the seamount chain, and their erosion is larger than 50 %. The other anticyclones are either completely eroded or trapped over a wide seamount top. Cyclones are less affected by seamounts because they oppose the topographic draft towards the seamount top and they drift along the side of the seamount. (4) Large vortices resist topographic erosion more efficiently. The rate of erosion grows from a few percent to about 35–50 % as the vortex radius decreases from about 60 to 30 km. Small cyclones are not eroded, contrary to small anticyclones (which completely decay), in relation with the different trajectories of these eddies in the vicinity of the seamounts. (5) The detailed vortex shape does not appear critical for their evolution, if they are close enough to the seamount chain initially. The interaction between a group of vortices initially north of the seamount chain can modify their trajectory to such an extent that they finally avoid collision with seamounts. (6) Finally, meddy trajectories across the Horseshoe Seamounts (data from the AMUSE experiment) show qualitative similarity with the vortex paths in the model. Several events of vortex decay also occur at comparable locations (in particular over the wide and tall seamounts) in the model and observations.

Keywords Meddies · Mediterranean Water cyclones · Vortex–seamount interaction · Horseshoe seamounts · RAFOS float data · Contour dynamics model · Vortex erosion and filamentation

Responsible Editor: Dirk Olbers

M. A. Sokolovskiy (✉) · B. N. Filyushkin
Water Problems Institute of RAS, 3 Gubkina Str.,
Moscow 119333, Russia
e-mail: mikhail.sokolovskiy@gmail.com

M. A. Sokolovskiy
Southern Federal University, 8a, Mil'chakova Str.,
Rostov-on-Don 344090, Russia

B. N. Filyushkin
P.P. Shirshov Institute of Oceanology of RAS,
36 Nakhimovskiy prosp.,
Moscow 117997, Russia

X. J. Carton
Laboratoire de Physique des Océans,
UFR Sciences, UBO, 6 Av. Le Gorgeu,
29200, Brest, France

1 Introduction

The Mediterranean Sea is an evaporation basin which forms salty water both in the Levantine Basin (Levantine Intermediate Water, LIW) and in the Gulf of Lions (Western Mediterranean Deep Water, WMDW). In the Alboran Sea, LIW and Upper

WMDW mix and fill a reservoir which pours out into the Gulf of Cadiz in the Atlantic Ocean, depending on the tidal conditions. In the eastern Gulf of Cadiz, the outflowing Mediterranean Water (MW) mixes with North Atlantic Central Water, as it cascades down the continental slope. This mixing leads to its density adjustment at depth, which is simultaneous with its northward deflection from the Straits of Gibraltar by the Coriolis force. In fact, the presence of different salinities in the outflow and the existence of canyons transverse to the continental slope lead to the formation of three undercurrents of MW, the coastal, the upper and the lower one, which settle at 450, 800 and 1200 m depth (Madelain 1970; Bower et al. 1997; Baringer and Price 1997; Johnson et al. 2002). The density adjustment is complete when the outflow has reached 8°W. The outflow trajectory is then westward and encounters the Portimao Canyon.

The canyons which indent the Iberian continental slope along the path of the MW outflow (Portimao Canyon, Cape Saint Vincent Canyon, Nazare Canyon) and the changes of orientation of the slope (at Cape Saint Vincent, Estremadura Promontory or at Cape Ortegal) destabilize this outflow (Ambar 1983; Armi and Zenk 1984; Käse and Zenk 1987; Bower et al. 1997; Aleynik et al. 1998; Paillet et al. 1999; Cherubin et al. 2000; Serra et al. 2002; Paillet et al. 2002). These topographic anomalies lead to the formation of anticyclonic lenses (Swallow 1969; Prater and Sanford 1994), often coupled with shallower cyclones (Filyushkin and Plakhin 1996; Aleynik et al. 1998; Carton et al. 2002; Ambar et al. 2008). These eddies are characterized by high temperature and salinity with respect to surrounding waters, with depth of maximal anomalies near the thermocline.

Observations indicate that the lifetime of cyclonic MW eddies does not exceed 0.5–1 yr, whereas anticyclonic MW eddies (called meddies) live 4–5 years on the average, but 4–6-year-old meddies were found in some cases (Yegorikhin et al. 1987). Geographically, cyclones have been observed mostly in the vicinity of the Iberian Peninsula (Filuyshkin and Plakhin 1996; Carton et al. 2002, 2010; see Fig. 1), whereas meddies have been observed as far as 30°W. Young meddies have two thermohaline maxima along their vertical axis, while older meddies possess only one anticyclonic core (Filuyshkin 1989). Meddies drift mostly westward and southwestward from their regions of formation, at irregular speed (1–3 cm/s on average, but up to 10 cm/s) (Aleynik 1998; Tychensky and Carton 1998) and up to 4,000-km distances (2,000–2,500 km on average). The mean currents and bottom topography are important factors for MW eddy drift (Morel 1995; Shapiro and Meschanov 1996; Morel and McWilliams 1997; Le Cann et al. 1999; Vandermeirsch et al. 2001; Filuyshkin et al. 2011b). Throughout their lives, meddies interact with their surroundings. Relatively slow erosion of MW lenses can result from the following mechanisms: (1) turbulent exchange with thermohaline intrusions at their external boundaries; (2) layerwise diffusive convection at their upper boundary; (3) double diffusion, forming salt fingers and staircases at the lower boundary (Fedorov 1978; Zhurbas and Kuzmina 1981). Meddy Sharon, which was monitored for 2 years (Armi et al. 1989; Richardson et al. 1989), slowly decayed under the effect of these processes. When this meddy was first located near the Azores front, its age was evaluated as 2 years. Then, the lens lost 2/3 of its heat and salt contents during about 300 days, and 1/3 in the following year.

In situ data in the Atlantic Ocean show that meddies propagating over seamounts can partially or completely decay (Dykhno et al. 1991; Shapiro et al. 1995; Richardson and Tychensky 1998; Richardson et al. 1999). Vortex–seamount interaction has been the subject of numerous studies. With a three-layer primitive-equation model, Herbette et al. (2003, 2005) found that the motion of deep fluid particles to and from an isolated seamount top generates a deep flow with an intense shear that can split an incoming anticyclone into two parts or more; it can also lead to its filamentation; part of the anticyclone can be advected away as a dipole with a deep cyclone; the important parameter for this interaction is the vorticity reservoir associated with the seamount top. With an equivalent barotropic model, Sutyrin (2006) showed that the anticyclonic vorticity generated over a narrow seamount top can deflect the incoming vortex westward, north of the topography; for a wide seamount, strong vortex erosion can be observed. With a three-layer primitive-equation model, Sutyrin et al. (2011) showed that a wide seamount which intrudes in the middle layer can lead to the horizontal or vertical splitting of the vortex core. With a barotropic model, Filyushkin et al. (2011b) found that a cyclone can drift along the northern periphery of an isolated seamount and then move away virtually unchanged, while an anticyclone can be divided into two unequal parts near such a topography, one part being captured by the seamount.

In the present work, we wish to investigate the role of a complex seamount chain on the drift and decay of intrathermocline eddies with a simple numerical model. Firstly, we recall observations of MW eddies interactions with the Horseshoe seamounts and their possible decay. Then, we use contour dynamics to model the evolution of deep eddies advected by mean currents over seamounts. The conditions were chosen to idealize MW eddies, regional mean flows and the Horseshoe seamounts with few parameters (Fig. 2). The initial position, size and intensity of the eddies were varied to determine their role in the eddy–seamount chain interaction. Finally, conclusions are drawn.

2 Observations of MW eddy interactions with the Horseshoe seamounts

The Horseshoe seamounts are shown on Fig. 2. The tallest ten of them are also identified. At least nine seamounts climb

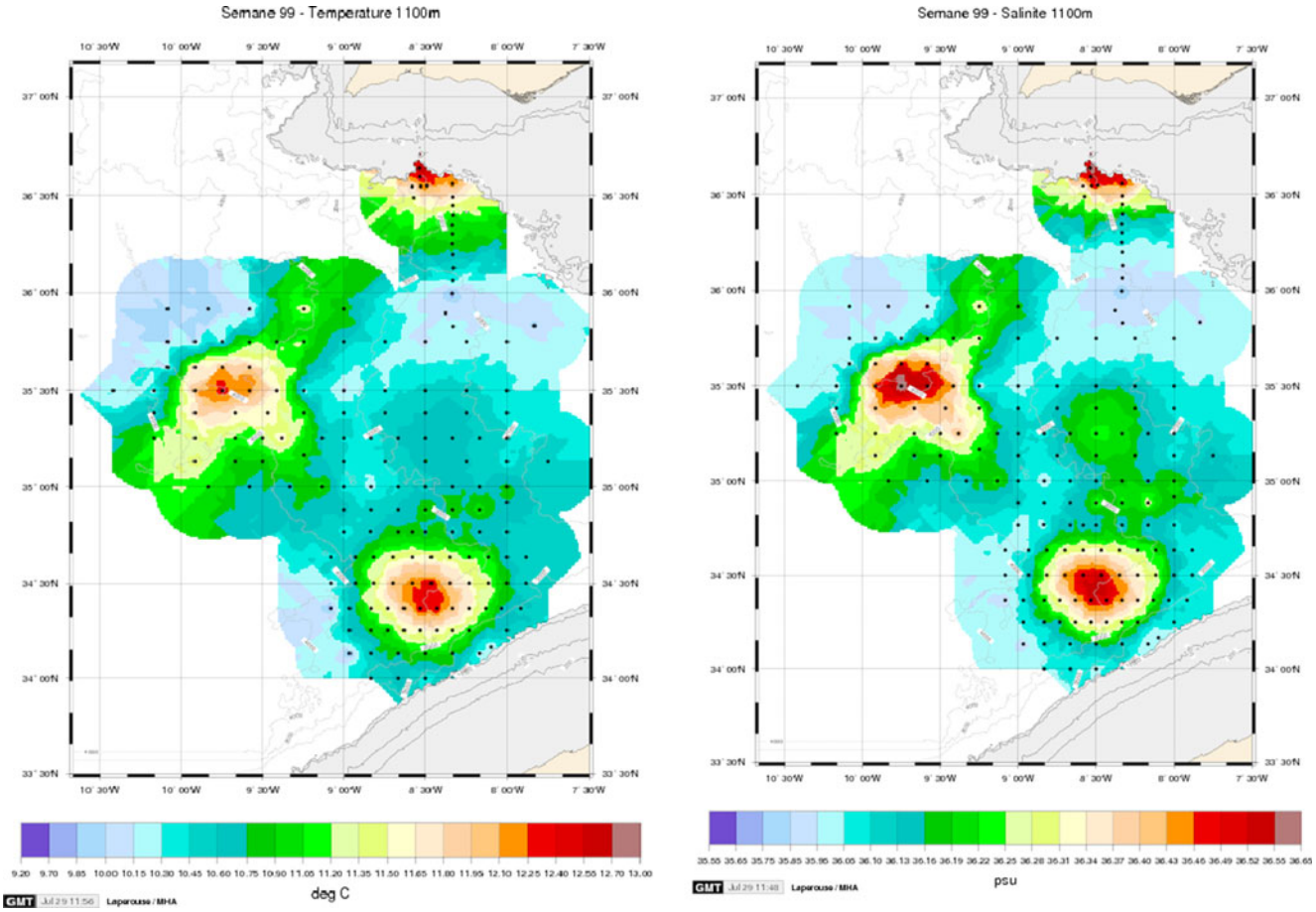

Fig. 1 Maps of temperature and of salinity at 1100 m depth in the Gulf of Cadiz as measured during the SEMANE 1999 experiment. To the north is the Portuguese continental slope and the South the Moroccan slope. Near the Moroccan slope lies a meddy; to its north lies a shallower cyclone of Mediterranean Water, and to the west of this cyclone lies another meddy. Near the Portuguese slope, the strong salinity anomaly is the MW outflow in the Portimao Canyon

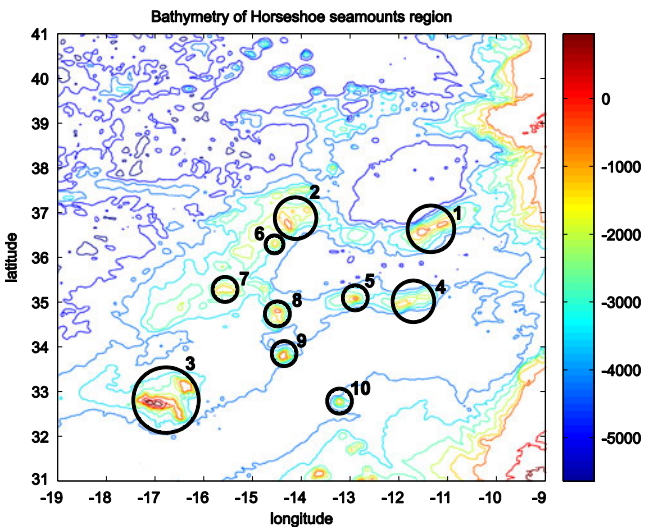

Fig. 2 Bathymetry of Horseshoe area (http://www.ngdc.noaa.gov/mgg/global/etopo2.html). The *circles* represent the boundaries of cylindrical seamounts, idealizing the most significant regional seamounts. Seamounts are numbered counterclockwise; first, the largest ones (1–4), and then the smallest ones (5–10)

higher than meddies depth (1100 m), and five mountains have their summits a few hundred meters below the ocean surface.

The regional currents form cyclonic gyres as indicated by prognostic or diagnostic models (Peliz et al. 2007; Alvez et al. 2011). A general ocean circulation model (Diansky et al. 2002) with 0.25 degree horizontal resolution and 27 vertical levels provided the currents at 1,000 and 1300 m depth in the Northeastern Atlantic Ocean (Filyushkin et al. 2008). The circulation pattern at 1,000-m depth indicates several gyres (see their Fig. 3b). One cyclonic gyre is located in the Gulf of Cadiz. Another cyclonic gyre is located essentially between 33 and 37°N and 10 and 15°W, with a northeast to southwest orientation. It mostly covers the Horseshoe seamounts. Another indication for the cyclonic motion southwest of Portugal was provided by Daniault et al. (1994) who found, from year-long measurements, a cyclonic recirculation of MW southwest of the Iberian Peninsula, with an average velocity of 7 cm/s but also with a strong mesoscale variability.

Though MW eddies may have a distinguishable signature in sea surface height or temperature, identifying MW eddies

with surface data only remains a challenge (Stammer et al. 1991; Tychensky and Carton 1998; Carton et al. 2010; Filyushkin et al. 2011a; Filyushkin and Sokolovskiy 2011; Bashmachnikov and Carton 2012; Bashmachnikov et al. 2013). Therefore, to trace MW eddy interaction with the Horseshoe seamounts, data from the in situ experiments, such as AMUSE (11.1993–04.1994) (Bower et al. 1997; Richardson et al. 1999), CANIGO (09.1997–09.1998) (Serra et al. 2002;

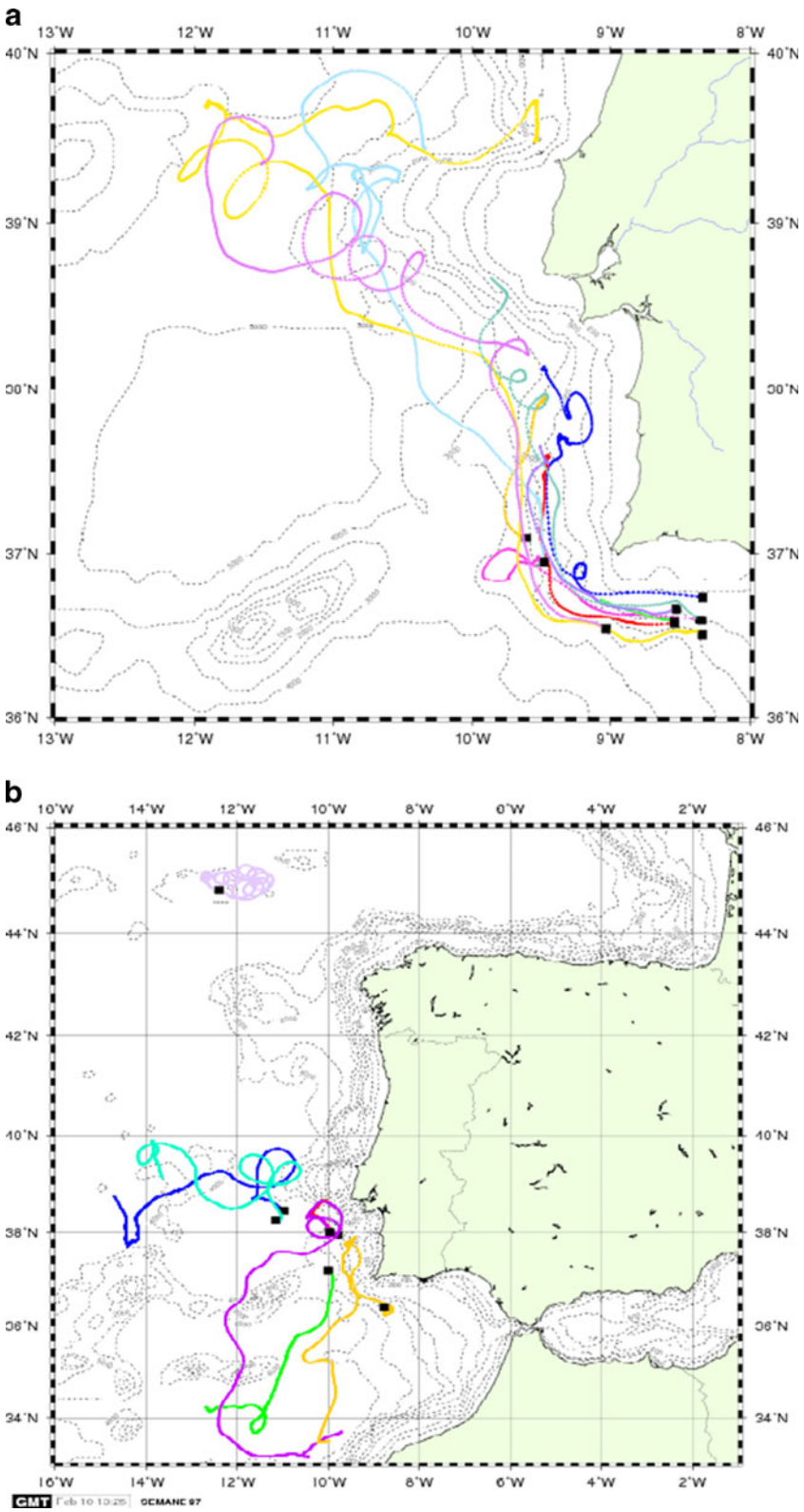

Fig. 3 **a** Trajectories of deep drogued Surdrift buoys of the SEMANE 1995 experiment seeded in Portimao Canyon, and near Cape Saint Vincent. The surface buoys were tethered to a 800- to 1200 m deep holey sock drogue via a thin Kevlar cable (with 2.5 mm thickness). The drift duration was at most 6 months (duration of the mission). Trajectories were terminated when the drogue was lost. **b** Trajectories of deep drogued Surdrift buoys of the Semane 1997 experiment seeded southwest of Portugal. The experimental conditions were similar to those of 1995 (see Fig. 3a). The meddy northwest of the Iberian Peninsula was described in Paillet et al. 1999, 2002

Serra and Ambar 2002), or other experiments (Filyushkin and Plakhin 1996; Aleynik et al. 1998; Carton et al. 2002) and from ARGO buoys in 2001–2010 Demidov et al. (2012) were used.

The RAFOS float database (the total duration is about 96 years) provided meddy trajectories and mean current in 1°×1° squares. The ratio of float trapping time in meddies to float drifting time in background currents was 1/3 (Sparrow et al. 2002). At 1,000-m depth, current vectors were calculated in 1°×1° boxes. The mean velocity in the coastal area was 6–12 cm/s, and it clearly decreased in the seaward direction.

Deep-drogued buoys of the SEMANE 1995 and 1997 experiments (Fig. 3) followed two main directions, one along the continental slope when they were trapped in the MW undercurrents, and one offshore when buoys were trapped in eddies or advected by the regional currents. In this latter case, the general motion was westward to south-westward, sometimes with a large-scale cyclonic motion.

Figure 4 adapted from Richardson et al. (1999) shows smoothed trajectories of 20 meddies identified and tracked during AMUSE or other experiments. The mean meddy velocity from their formation up to their destruction was about 2 cm/s in the direction 227°.

During the AMUSE project, 85 RAFOS floats were launched in the 800–1200 m depth range either in the MW undercurrents or in previously found MW eddies (Bower et al. 1997). Three meddies (5, 9, 13 on Fig. 4) were continuously tracked during 1 year, and two of them (4, 6) for about 1.5 years (Bower et al. 1997; Richardson et al. 1999). Six meddies were initially observed, already completely formed, near Cape Saint Vincent (7, 8, 9, 14, 18, 20), and three meddies in the vicinity of the Estremadura Promontory (10, 16, 17).

Meddies (4, 6 and 9) drifted significantly north of the Horseshoe seamounts. These eddies conserved their volume while drifting across the ocean. Another meddy group (5, 11, 13, 15–19) located between the Josephine and Gorringe banks drifted to the southwest into the internal area of the Horseshoe seamounts, where part of them decayed after colliding with the seamounts. Meddy 5 drifted from 11.93 until 02.94 between the seamounts; then, the float signal disappeared. The same situation occurred with meddies 11 and 15–19. Meddies (3, 12, 16) were stationary during the whole period of observations. In summary, about 69 % of all meddies tracked with these floats collided with seamounts, decayed partially or totally, and only 31 % of them, after crossing this system of seamounts, arrived in the Canary Basin (Richardson et al. 1999).

The frequent collisions of meddies with seamounts and their further decay cause temperature and salinity increase at intermediate depths in this area. The average lifetime of meddies also decreases locally; it was evaluated as only 1.7 years (Richardson et al. 1999).

These data allow us to formulate conditions for model experiments idealizing the observed situation. We take into account ten seamounts, and a cyclonic large-scale current. We assume that meddies can start from various locations north of the seamounts. The main question addressed with these experiments is "how does this complex seamount chain form a barrier to the propagation of these eddies and how is it involved in their decay?"

3 The physical and numerical model

We use a three-layer quasi-geostrophic model on the *f*-plane (we neglect the planetary beta effect in consideration of the limited meridional extent of our domain and of the prevalence

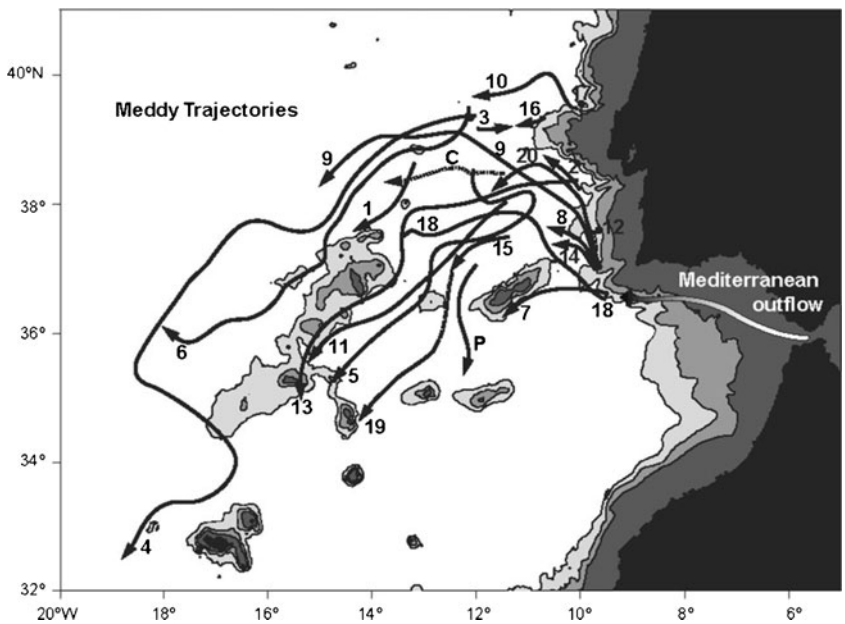

Fig. 4 Trajectories of 20 Iberian-basin meddies in the North Atlantic (Richardson et al. 1999, Fig. 2b). The description is given in the text

of the topographic effect). The eddies are represented here as initially circular patches of uniform potential vorticity in the intermediate layer. The equation governing potential vorticity (PV) in the quasi-geostrophic model on the *f*-plane is (Kamenkovich et al. 1986).

$$d_i q_i \Big/ dt = 0,$$

Where i=1, 2, 3 being the upper, intermediate and lower layer indices, and

$$\begin{aligned} q_1 &= \nabla^2\psi_1 + F_1(\psi_2-\psi_1)/H_1, \\ q_2 &= \nabla^2\psi_2 + F_1(\psi_1-\psi_2)/H_2 + F_2(\psi_3-\psi_2)/H_2, \\ q_3 &= \nabla^2\psi_3 + F_2(\psi_2-\psi_3)/H_3 + f_0\sigma/H_3. \end{aligned}$$

Here, $\nabla^2=\partial^2/\partial x^2+\partial^2/\partial y^2$ and $d_i/dt=\partial/\partial t+u_i\partial/\partial x+v_i\partial/\partial y$ are the 2D Laplace operator and the total time derivative; $F_1={f_0}^2/{g_1}'$ and $F_2={f_0}^2/{g_2}'$ are based on the reduced gravity between layers 1 and 2, and 2 and 3, respectively. The Coriolis parameter is f_0, the topographic height is σ.

The numerical model is based on the Contour Dynamics Method (Sokolovskiy 1991), with the procedure of Contour Surgery (Makarov 1991). Each patch of uniform PV is bounded by a contour discretized with nodes. These nodes are advected by the flow generated by the potential vorticity patches. Contour separation or reconnection occurs when the local curvature exceeds a given threshold. Renoding of the contours is also achieved to maintain a fixed density of nodes on each contour during its deformation. Contours are deleted when they become smaller than a prescribed size. In such codes, area integral of potential vorticity is conserved quite accurately in the absence of destructive or erosive PV patch interaction.

The total ocean depth is H=4000 m, the upper, intermediate and bottom layer thicknesses are H_1=600 m, H_2=1000 m and H_3=2400 m (dimensionless thicknesses are h_1=0.15, h_2=0.25, h_3=0.6); the first and the second deformation radii are Rd_1=32 km, Rd_2=15 km which allows the computation of the Froude numbers F_1 and F_2, via the eigenvalues λ_i of the stratification matrix (Sokolovskiy 1991):

$$\lambda_1 = 0; \quad \lambda_{2,3} = -\frac{1}{2}\left[\frac{F_1}{h_1}+\frac{F_1+F_2}{h_2}+\frac{F_2}{h_3} \mp \sqrt{\left(\frac{F_1}{h_1}+\frac{F_1+F_2}{h_2}+\frac{F_2}{h_3}\right)^2 - 4\frac{F_1F_2}{h_1h_2h_3}}\right], \quad \left(R\Big/Rd_{1,2}\right)^2 = -\lambda_{2,3}, \tag{1}$$

where R is a characteristic horizontal scale. Taking into account the parameters listed above, and assuming $R=Rd_1$ =32 km, we obtain F_1=0.14, F_2=0.7378. Therefore in our model, the vortices having unit dimensionless radius in the basic configuration correspond to oceanic eddies with radius R=32 km. In this work, we study processes that have horizontal scale of few Rossby radii; thus, the use of *f*-plane approximation is justified. Furthermore, the advection of vortices by the mean flow or by topographic effects is stronger than a beta drift would be, and vortex deformation and erosion due to topography is also stronger than dispersion that would be created by Rossby waves.

To the vortex flow, a large-scale barotropic current is added with stream function

$$\Psi = \frac{A}{2}\left[Bx^2 + (1-B)y^2\right] \tag{2}$$

For B=0 or B=1 zonal or meridional shear currents are obtained, correspondingly. For $0<B<1$, an elliptical point lies at the origin of the plane, and for $B>1$ a hyperbolic point; in our calculations, we assume B=0.5. Parameter A defines the velocity scale: A=1 corresponds to a velocity of 50 cm/s. In the absence of bottom topography, vortex drift is completely determined by the large-scale barotropic flow (Fig. 5a). In this experiment, it is assumed that A=0.2, i.e. a velocity scale V=10 cm/s. The vortex moves along a circle with dimensionless radius R=17.26 (or 558.72 km as the horizontal scale is the first Rossby deformation radius, 32 km). The half circumference followed by the vortex lasts about 30 units of dimensionless time. Here, the time scale is T=6.77 days.

The seamounts are represented by cylinders (see also Wang and Dewar (2003)), i.e. we set

$$\sigma = 0.1\sum_{j=1}^{10}\sigma_j\Theta(S_j),$$

Where $\Theta(S_j)$ is the Heaviside step function equal to 1 inside the circle domains S_j and equal to 0 outside them. Vortex–seamount interaction models have shown that the detailed shape of the seamount is of secondary importance compared to the seamount volume (Kozlov 1983). Moreover, calculations with a barotropic model have shown only very small differences in the response of the flow to "cylindrical" versus "Gaussian-shaped" obstacles (Sokolovskiy et al. 1998). Here, all seamounts are confined in the lower layer (that is, below 1600 m depth). We can also note that such idealized seamounts influence the dynamics of the vortices in the intermediate layer less directly than if they were located in a barotropic flow.

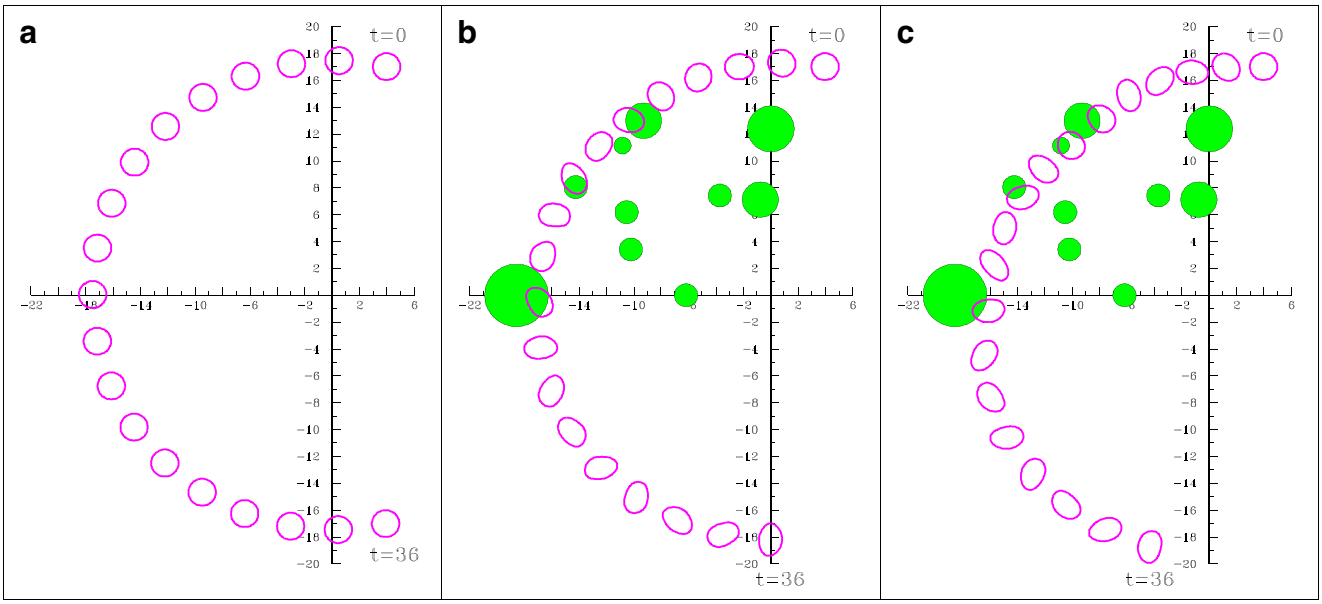

Fig. 5 Successive positions of the anticyclonic eddy contour (*lilac lines*) in the dimensionless time interval [0; 36] with time step 2. The initial position is $(x_0, y_0)=(4, 17)$: **a** evolution over flat bottom; **b** evolution of seamounts with heights reduced tenfold; **c** evolution of seamounts with heights reduced fourfold. Filled green circles represent seamounts in top projection

The seamounts have the following dimensionless centers: $(x_j, y_j)=(0.0, 12.39)$; $(-9.29, 13.00)$; $(-18.58, 0.0)$; $(-0.77, 7.22)$; $(-3.72, 7.43)$; $(-10.88; 11.55)$; $(-14.25, 8.05)$; $(-10.53, 6.19)$; $(-10.22, 3.41)$; $(-6.19, 0.0)$, $j=1, 2, \ldots, 10$. So, the coordinate origin coincides with (x_1, y_3). Their relative heights and radii are the following: $(\sigma_j, r_j)=(2.76, 1.7)$; $(3.44, 1.32)$; $(1.85, 2.32)$; $(2.5, 1.32)$; $(4.16, 0.85)$; $(5.20, 0.62)$; $(2.76, 0.85)$; $(4.16, 0.85)$; $(4.16, 0.85)$; $(2.76, 0.85)$.

4 Numerical experiments

4.1 Influence of the mean flow and of the seamount characteristics

We investigate different cases of vortex interactions with the seamount chain. In a first series of experiments, the vortex centers are initially located at latitude $y_0=17$. Note that, for flat bottom (and $B=0.5$), the streamlines of (2) are concentric circles around the center of the plane. Figure 5a confirms this: over flat bottom, the anticyclonic vortex rotates under the influence of cyclonic barotropic circulation ($A>0$), barely changing its shape. Figure 5b, c shows that the seamounts affect the cyclonic motion and amplify the vortex deformation. In this figure and in the following ones, the vortex contours are represented at several non-dimensional instants.

As Fig. 6 shows, the seamounts affect the mean flow in all layers. The mean flow is the sum of the barotropic, cyclonic large-scale current, and of the baroclinic, anticyclonic circulation which forms over the seamounts due to potential vorticity conservation. The topographic circulation is the strongest in the bottom layer. Comparing panels *(a)* and *(b)* of Fig. 6, the influence of topography is larger for faster cyclonic mean flow. Comparison of panels *(b)* and *(c)* shows that taking into account smaller seamounts affects the specific structure of the phase plane (number of hyperbolic points, size and number of isolated regions), though the large-scale structure of the streamlines remains similar in all layers.

In further numerical experiments, the "external field" will be that shown in panel *(b)*. The vortex presence distorts the streamlines (see Fig. 9 for instance), but the phase plane described above will be useful to explain the vortex dynamics, as we will show below.

4.2 Influence of the initial vortex position

In Fig. 7, we show the results of three numerical experiments simulating the effect of an external field on an anticyclonic lens of unit radius (in dimensional variables its radius is equal to 32 km), the center of this lens is initially located at points **a** (lilac contours), **b** (blue contours) and **c** (red contours), respectively (three different cases). Note that each experiment was carried out independently. In this figure, the different colored contours are superimposed artificially at several non-dimensional instants.

When $x_0=-16$ (the lilac contours), the anticyclonic vortex initially lies to the west of all seamounts, except seamount **3**. The vortex trajectory mainly follows the regional cyclonic flow. When approaching seamount **3**, the vortex contour is deformed by the topographic flow. Then, a small

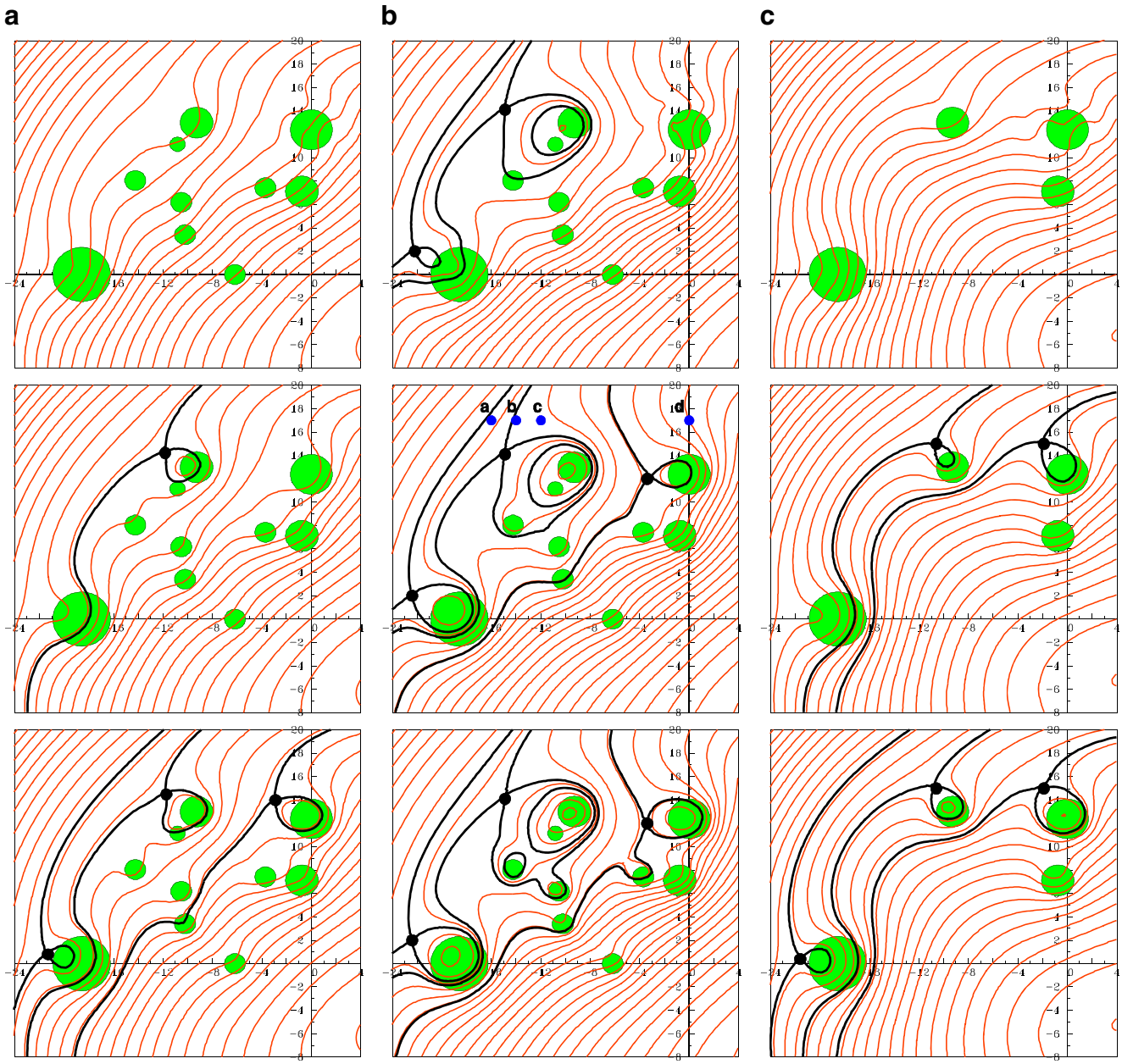

Fig. 6 Streamlines of the total mean flow in the upper, middle and bottom layers (from *top to bottom*), for B=0.5, and A=0.1 (**a**), or A=0.2 (**b**, **c**). In column (**c**) only the largest seamounts (1–4) are taken into account. The *green disks* represent the cylindrical seamounts (viewed from the *top*), located in the bottom layer. The *thick black lines* represent the separatrices, separating areas with different topological properties of the streamlines. Topographic capture zones are located inside loops, where stationary anticyclonic eddies can exist; they are localized over separate seamounts or parts of seamounts. The *black dots* indicate hyperbolic points (self-crossing of the separatrix). *Blue dots* with letters **a**, **b**, **c**, **d** correspond to the initial positions of eddy centers in the following numerical experiments (Figs. 7, 8, 9, 10, 11, 12, 13, 14, 15, 16)

part of this vortex is captured by the seamount, but the larger part is carried away by the flow. This evolution is qualitatively predicted by Fig. 6b because the initial position of the vortex center (point **a**) and the phase trajectory in the "external field" belong to the area of the transit current between two separatrices.

A small eastward displacement of the initial vortex position (x_0=−14, blue contours) results in a slowdown of the initial cyclonic motion of the vortex; seamount **3** strongly influences the vortex, the largest part of which is captured by this topography. The difference between the second and the first experiments is that the ratio of the lens volume trapped by seamount **3** and the total volume of all the vortex remnants is significantly larger in the second experiment. Considering the advecting flow from both initial positions (see again Fig. 6b), a larger difference in vortex trajectories

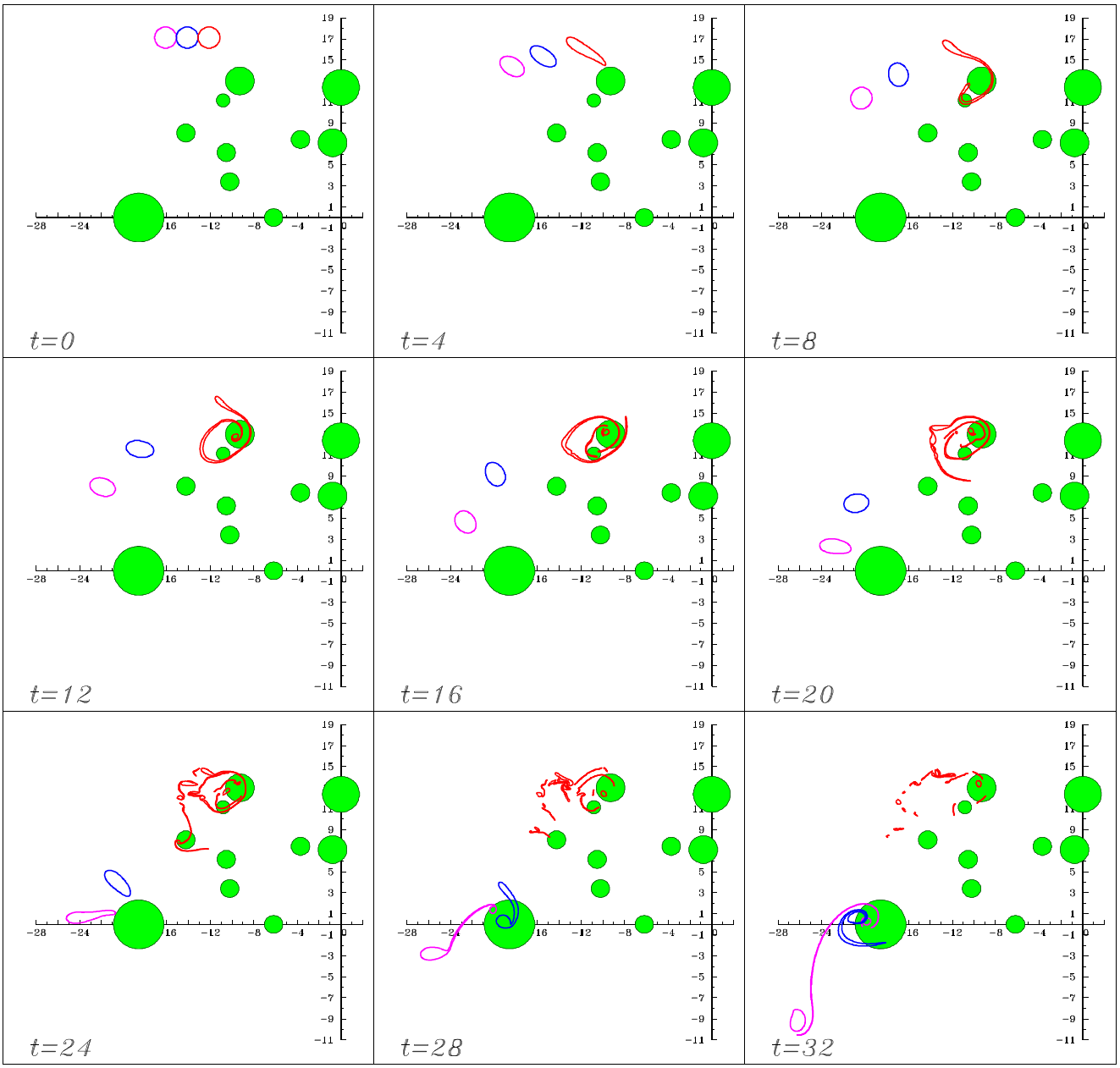

Fig. 7 Successive states of an anticyclonic eddy boundary in the intermediate layer of the model, at non-dimensional times indicated, for a mean flow with B=0.5, A=0.2 and for the initial eddy longitudes x_0=−16 (*lilac lines*, point **a** in Fig. 6b), x_0=−14 (*blue lines*, point **b** in Fig. 6b) and x_0=−12 (*red lines*, point **c** in Fig. 6b). These three different cases are artificially superimposed at each instant in this figure

between these two experiments would be expected, as points **a** and **b** lie near two successive separatrices of the external flow (though this latter differs from the total flow due to the presence of the vortex in the intermediate layer). Figure 8.1 presents the streamlines of the total flow at two instants for an anticyclonic vortex initially at point **b**. Figure 8.1.a shows that the vortex flow shifts both separatrices to the right. In both cases, this flow affects the possible vortex motion along the western side of the mountain ridge. Though the motion is unsteady (and therefore the streamlines do not coincide with the particle trajectories), the closed areas inside the separatrices indirectly characterize the vortex patch capture zones, as seen in Fig. 8.1.b at time t=32.

The following experiment (x_0=−12, red contours in Fig. 7) exemplifies a different situation. Here, topography strongly affects the vortex trajectory from the beginning, as shown by an early anticyclonic motion. Thus, the vortex heads very quickly towards seamount **2**; the vortex is totally captured by this seamount and by the adjacent seamount **6**. During this interaction, the vortex disintegrates into small

vortices and filaments. In this case, the northern part of the seamount chain is an insurmountable obstacle to the vortex propagation. A qualitative explanation of this effect can be obtained from Fig. 8.2: nearly the whole vortex is trapped inside the closed area.

Displacing the initial vortex position to x_0=0 (Fig. 9 and point **d** in Fig. 6b) renders the vortex substantially influenced by seamounts **1**, **4**, **5**, **9** and **3**. In the final stage of the experiment, 6.4 % of the lens original volume is captured by seamount **1**; 6.6 % remains in the vicinity of seamount **9**; 47.3 % of the volume is carried by the regional flow south of the ridge, and 39.3 % is lost when passing over the seamount chain. Hereafter, when examining the influence of different parameters on the vortex evolution, we will consider case **d** as a reference.

4.3 Influence of vortex size and shape

Figure 10 shows the results for case **d**, when the initial anticyclonic vortex is circular and has a radius twice as large (i. e. equal to 2 in non-dimensional variables, or to 64 km in the ocean). Such a vortex crosses the seamount chain without much alteration: after the interaction with seamounts **1**, **4**, **5**, **9** and **3** (at the end of the calculation), it has lost only 0.32 % of its volume; 91.17 % of this volume is concentrated in a relatively compact core and 8.51 % in the filaments.

The following two experiments allow us to examine the role of the initial vortex shape on its subsequent topographic interaction and erosion. Figures 11 and 12 present cases where the initial vortex is an ellipse with the same volume as in the previous case (see Fig. 10). The aspect ratio of

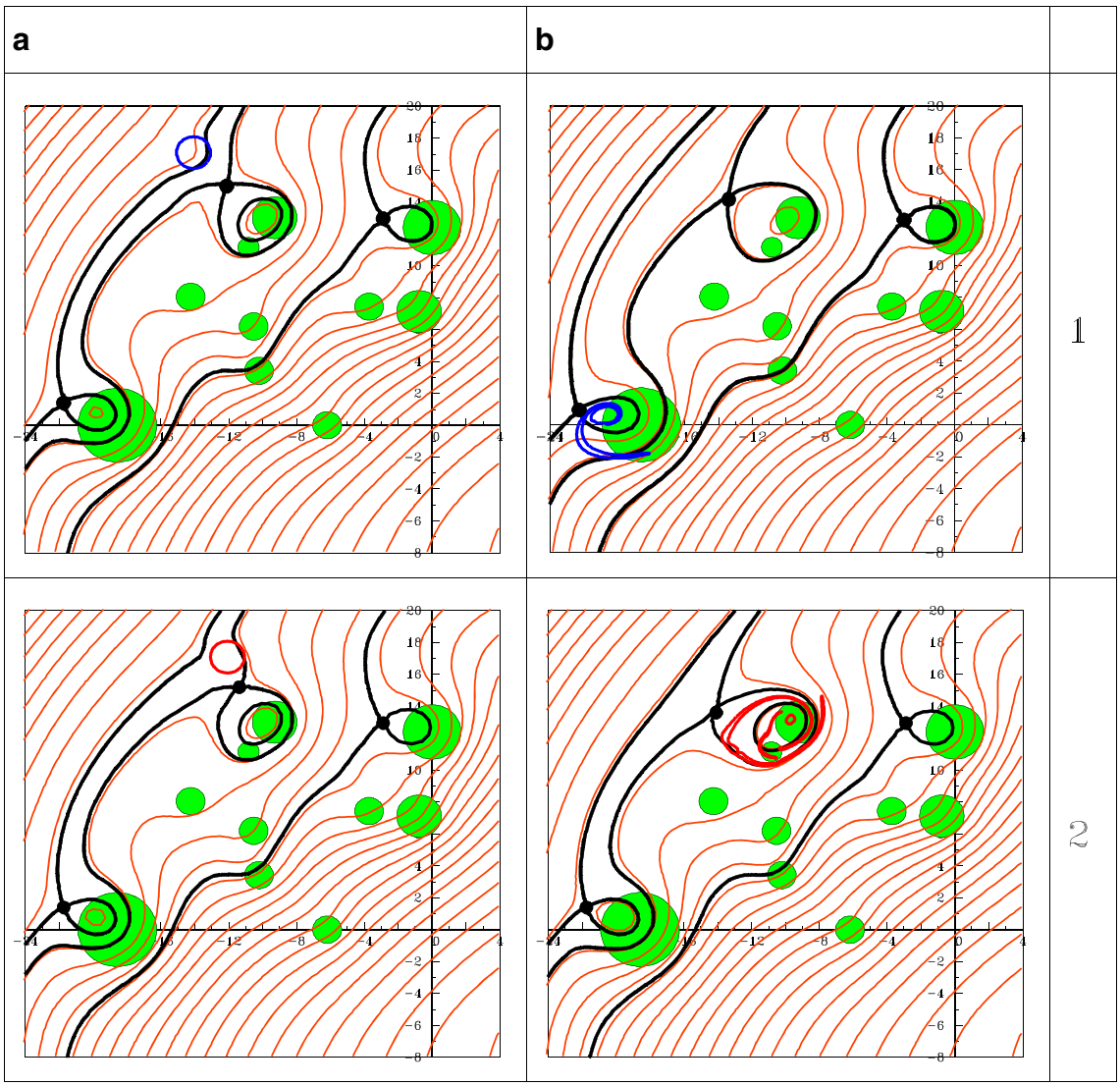

Fig. 8 Streamlines in the intermediate layer in presence of meddies. **1** the eddy initial position is in the point **b**, **2** the eddy initial position is in the point **c**; (*a*): t=0, (*b*): instantaneous vortex positions and boundaries at t=32 (row **1**) and t=16 (row **2**)

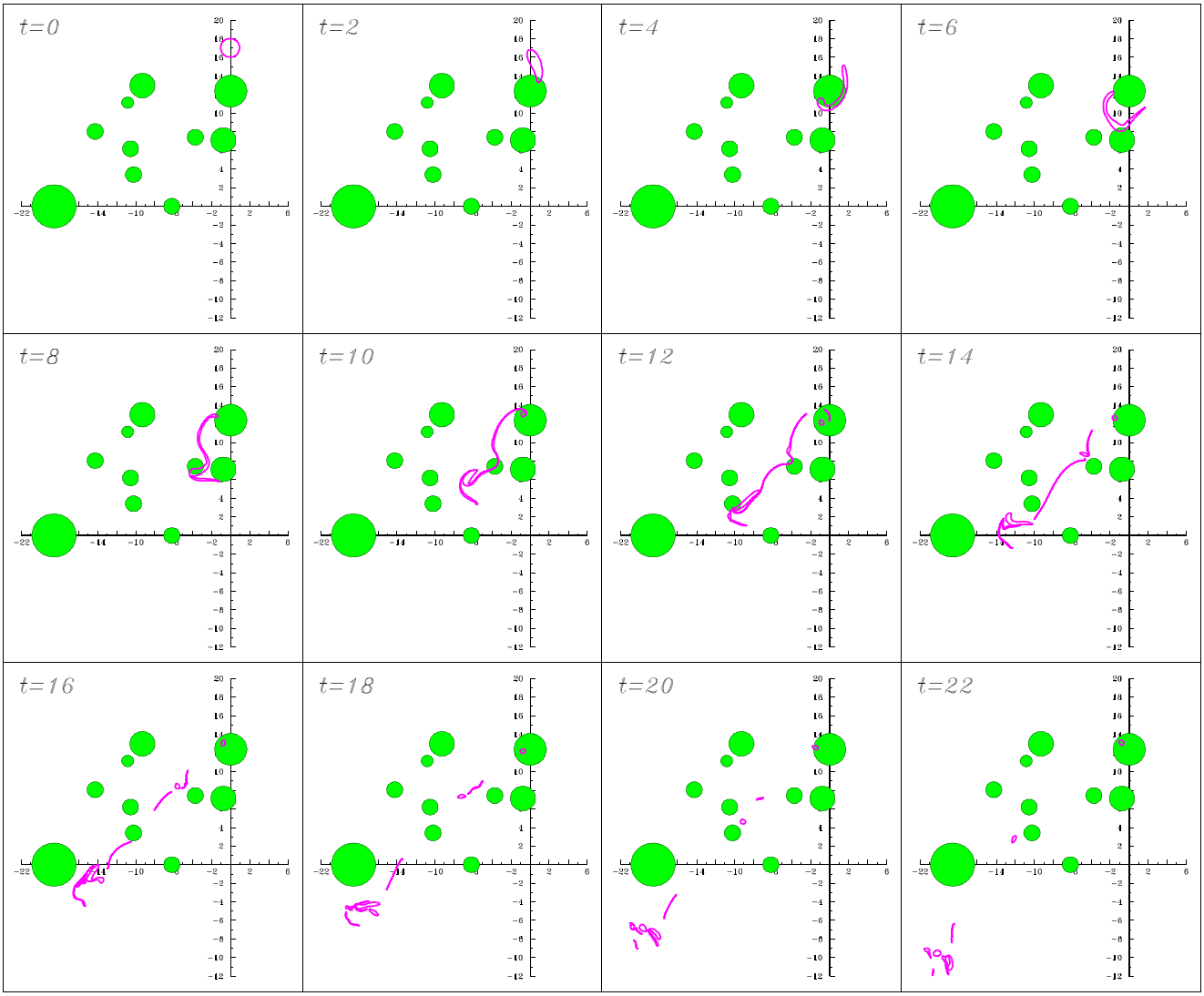

Fig. 9 Successive states of an anticyclonic eddy boundary (*lilac line*) in the intermediate layer of the model, at non-dimensional times indicated, for a mean flow with B=0.5, A=0.2 and for the initial eddy longitude x_0=0 (point **d** in Fig. 6b)

these ellipses is equal to $\chi=a/b=5.4$ in the first case and to $\chi=10$ in the second case. The choice of these values of χ was dictated by stability calculations (see Filyushkin and Sokolovskiy 2011): starting from $\chi=5.4$ an isolated elliptical vortex divides into two equal parts, and at $\chi=10$ into three parts. Here, this slow splitting of the ellipses is considerably perturbed by the "strong" external field. In particular, in the presence of topography, the vortex rapidly wraps up around seamount **1**, a process which prevents its natural splitting and which gathers a substantial part of its volume once the vortex detaches from the seamount. These experiments show qualitatively that the outcome of vortex seamount chain interaction only weakly depends on the initial shape of the vortex (provided it is initially close enough to the topography). In both cases, large parts of the vortices leave the seamount chain along nearly the same trajectory. The most significant difference concerns the more elongated shape and the longer life of filaments for initially elliptical vortices. At the end of the numerical experiment with $\chi=5.4$, 0.87 % of the initial vortex volume is lost, and at $\chi=10$ the loss is equal to 1.89 %. Thus, using circular vortex shapes in the calculations suffices to reproduce the main features of the interaction of more complex vortices with the seamount chain.

4.4 Dynamics of the vortex structures

We consider now a more complicated case, where not one, but several vortices are initialized near the seamount chain. Let three circular anticyclonic vortices of unit radius be originally located at points **a**, **c** and **d**. Below, in Figs. 13,

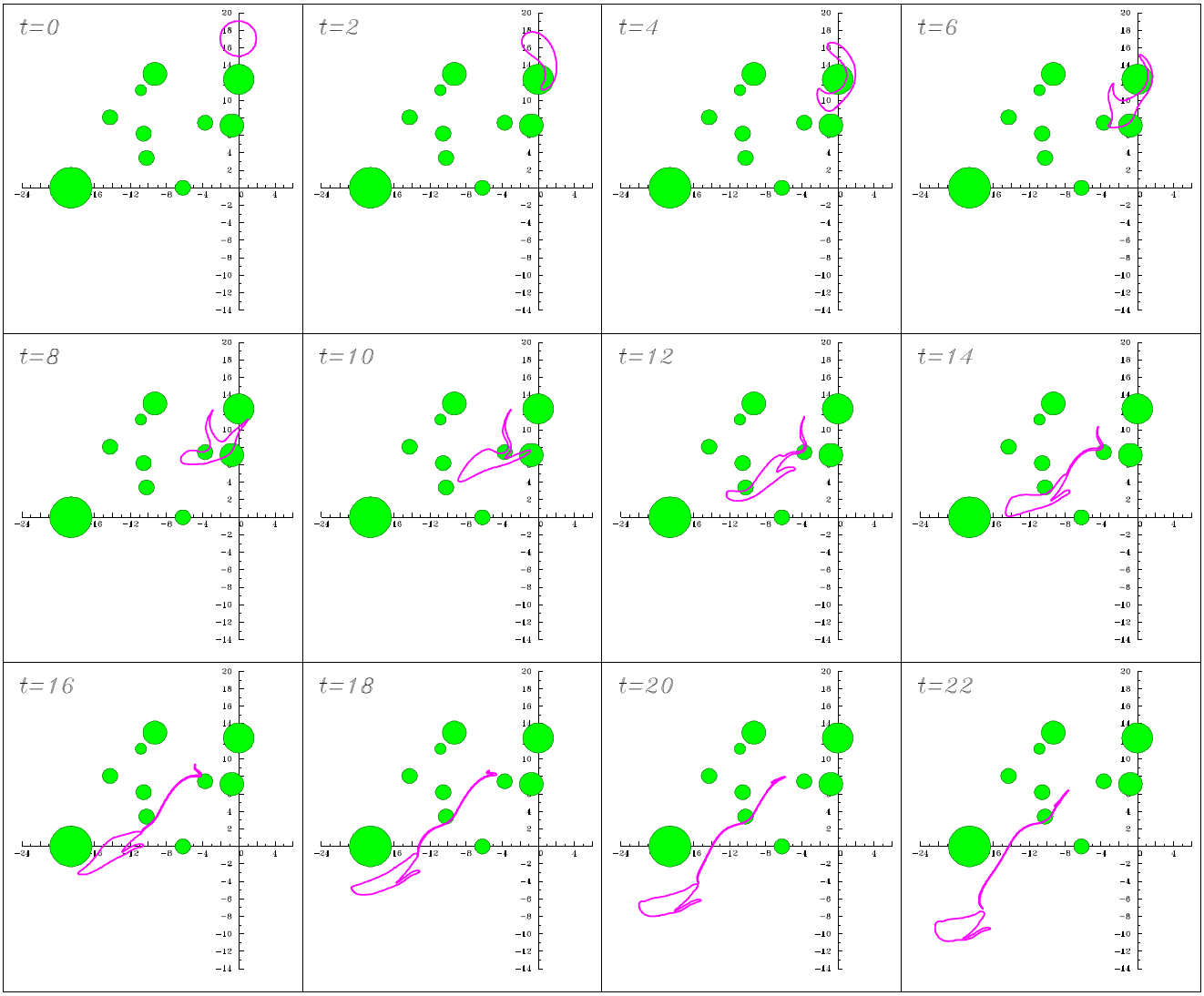

Fig. 10 Same as Fig. 9, but for an eddy twice as large (point **d** in Fig. 6b)

14, 15, the differently colored vortices interact because they are present simultaneously in the flow, unlike Fig. 7.

Figure 13.1 shows the early evolution of such a vortex group, initially collinear, in the absence of topographic influence (the shaded circular area at the location of Horseshoe Mounts plays here a scaling role): (*a*) represents a free state, and (*b*) the state when an external flow of the form (2) with A=0.2 and B=0.5 is present. Free vortices, separated by a large distance, behave like point vortices. On the contrary, two vortices, located closer to each other, rotate with respect to an instantaneous local center (Fig. 13.1.a). The whole system consisting of three vortices rotates slowly in the anticyclonic direction around its center, but the initially easternmost vortex is less affected by this global motion. Figure 13.1.b shows the initial motion of the same vortices, but in the presence of the regional cyclonic circulation (with the same parameters as before). The vortex interaction is weak here because of the dominant influence of the external flow. The same result holds for three cyclonic eddies (Fig. 13.2). In this case, the vortex interaction leads to a counter-clockwise rotation, but again the external flow is dominant.

Adding of the topographic features (Figs. 14 and 15, for the same vortices, anticyclonic and cyclonic, correspondingly) increases again the external flow effect. However, even weak vortex–vortex interactions can lead to qualitative changes in vortex–topography interactions.

Indeed, comparing the motion of the group of vortices issued from points **a**, **c** and **d** (see Fig. 14), with the motion of each single vortex (Figs. 7 and 9) displays only minor changes for cases **c** and **d** but a qualitative difference for case **a**: because of its weak, but continuous deviation in the anticyclonic direction, the three-vortex group does not come in close contact with seamount **3** and keeps its high compactness during the whole numerical experiment. For the group of three cyclonic vortices (Fig. 15), the vortex–vortex

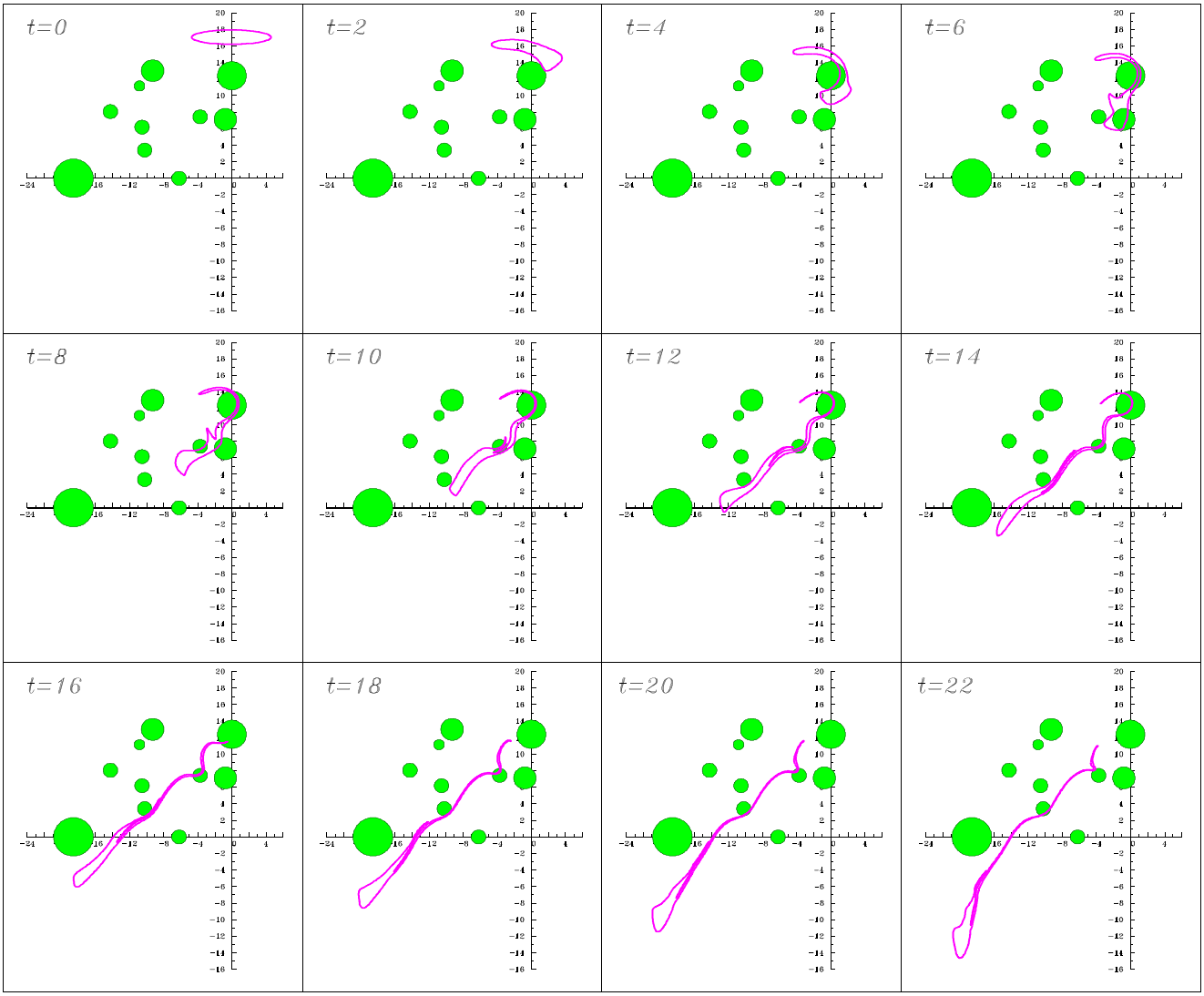

Fig. 11 Same as Fig. 10, but for an elliptic eddy with χ=5.4 (point **d** in Fig. 6b)

interaction is even more beneficial to the vortex survival. The deviation of the westernmost vortex favors its drift towards, and connection with, seamount **3**. The vortex is temporarily captured by the seamount, but eventually leaves its neighborhood. This eventual escape is related to the cyclonic nature of the vortex group. In the final state, the cyclones have been less eroded than the corresponding anticyclones. It was demonstrated in Filyushkin and Sokolovskiy (2011) and Filyushkin et al. (2011b) that cyclonic vortices, commensurate with the Rossby radius of deformation, interact less intensely with submerged obstacles than anticyclonic ones.

Note that in a relatively strong external field the evolution of the vortex structures is always "slow". That is why in the experiments with elliptical vortex patches (Figs. 11 and 12) their instability did not have enough time to grow before the vortex shape changed significantly in the external deformation field.

4.5 Influence of the vortex polarity on its topographic decay

Figure 16 shows the time evolution of the vortex area, from its initial state to the largest fragment in the final state. Here, we consider anticyclones and cyclones initially located at point **c**, which significantly decay and are completely captured by a mount. We also vary their size. They have initial radii 0.5 Rd, Rd, 1.5 Rd, 2.0 Rd. The loss of volume of anticyclones is respectively 100, 48, 22 and 3 %. Cyclones lose only 0, 34, 24 and 8 % of their volume. When crossing the seamount chain, the cyclones more efficiently survive the topographic perturbations. In this case also, large anticyclones survived more efficiently than small anticyclones. But the survivability of the vortex is not equivalent to its ability to cross the seamount chain. Most often, vortices drifting across the chain undergo trapping or nearly complete erosion as was shown above.

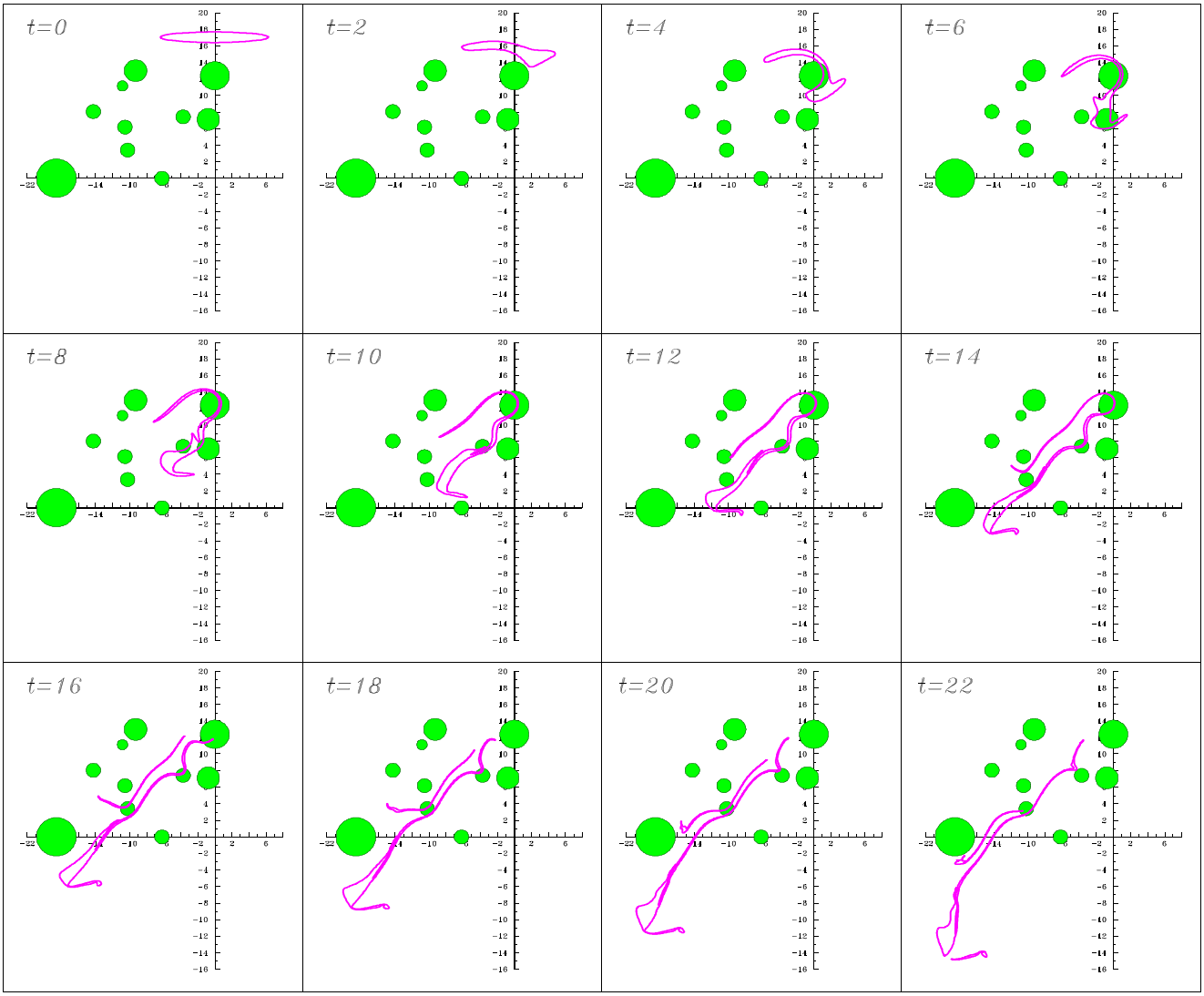

Fig. 12 Same as Fig. 10, but for an elliptic eddy with χ=10 (point **d** in Fig. 6b)

5 Discussion and conclusion

In the framework of a three-layer quasi-geostrophic model and using the simplest elements of topography and of external flow, we carried out contour dynamics simulations of vortex evolution in the intermediate layer. The novelty of this study was the complex distribution of the seamounts in the chain, as well as the number of initial situations considered (some involving several vortices).

Though the model settings are idealized compared to reality, the numerical simulations led to several conclusions which can be of interest to compare with in situ observations. In detail, the main findings are the following:

1. Though they represent only the steady part of the flow, the streamlines of the barotropic regional flow and of the baroclinic topographic flow are a useful tool to predict the fate of the eddies (see also Sutyrin et al. 2011): they describe which initial conditions can lead to encounter with seamounts, where stronger velocity shears will occur, therefore leading to erosion. Obviously, the real flow at every instant also includes the vortex contribution and that of its interaction with the topographic and regional flows. Also, the flow in the intermediate layer does not directly reflect the flow in the lower layer (but only its contribution via vortex stretching). In particular, the topographic flow is stronger in the lower layer than in the intermediate layer.
2. In that respect, the tallest and widest seamounts which have the largest vorticity reservoir generate the largest topographic flow and thus velocity shears. They are able to considerably erode the incoming vortices, but also, in

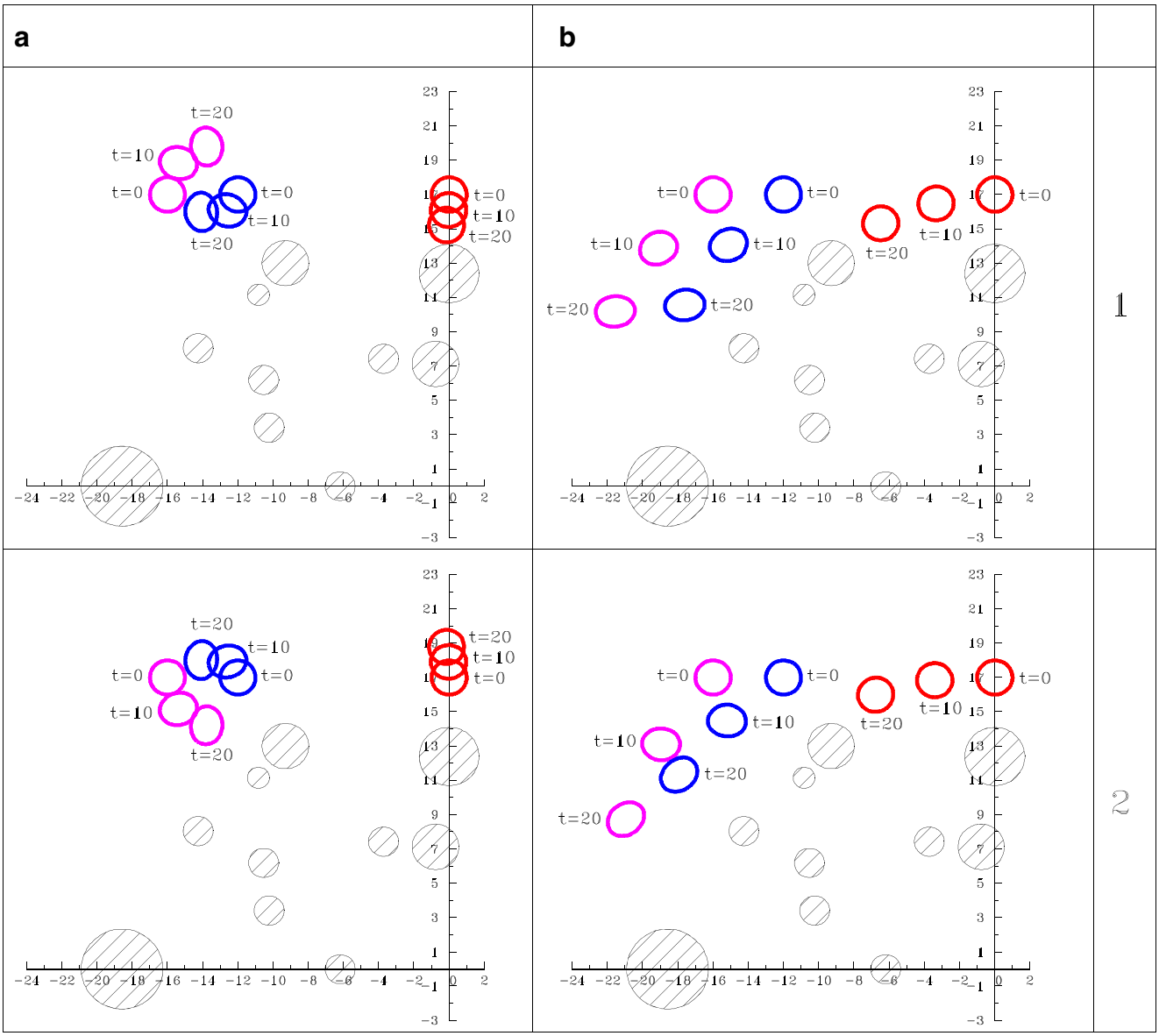

Fig. 13 Initial stages of motion of originally collinear structures composed of three vortex patches which start from the positions **a** (*lilac line*), **c** (*blue line*) and **d** (*red line*) when topographic disturbance is absent. **1**: anticyclonic vortices; **2**: cyclonic vortices; **a** free vortices; **b** vortices in the cyclonic gyre of type (2)

the unsteady evolution, to draw anticyclones towards the seamount top. The ability of narrower seamounts to completely erode vortices is related to their multiplicity: a vortex which is stretched by a first seamount can be split by the following one, whereas this would not occur for an isolated seamount. For anticyclones with radii equal to the first internal deformation radius (32 km), a series of experiments (not completely shown here) led to the conclusion that only 1/3 of the vortices reached the southern boundary of the seamount chain, and that their erosion was larger than 50 %. The rate of survival was naturally larger for the initially westernmost or easternmost vortices. The other anticyclones were either completely eroded or their remnant was trapped over a wide seamount top. Cyclones were less affected by seamounts because they opposed the topographic draft towards the seamount top and they drifted along the side of the seamount. Therefore, their erosion was weaker than that of anticyclones and their survival rate was larger. But they could remain trapped between two seamounts. Therefore, their rate of escape from the seamount chain was not much larger than that of anticyclones.

3. Initially larger vortices (as well as stronger ones) obviously resist more efficiently the topographic erosion.

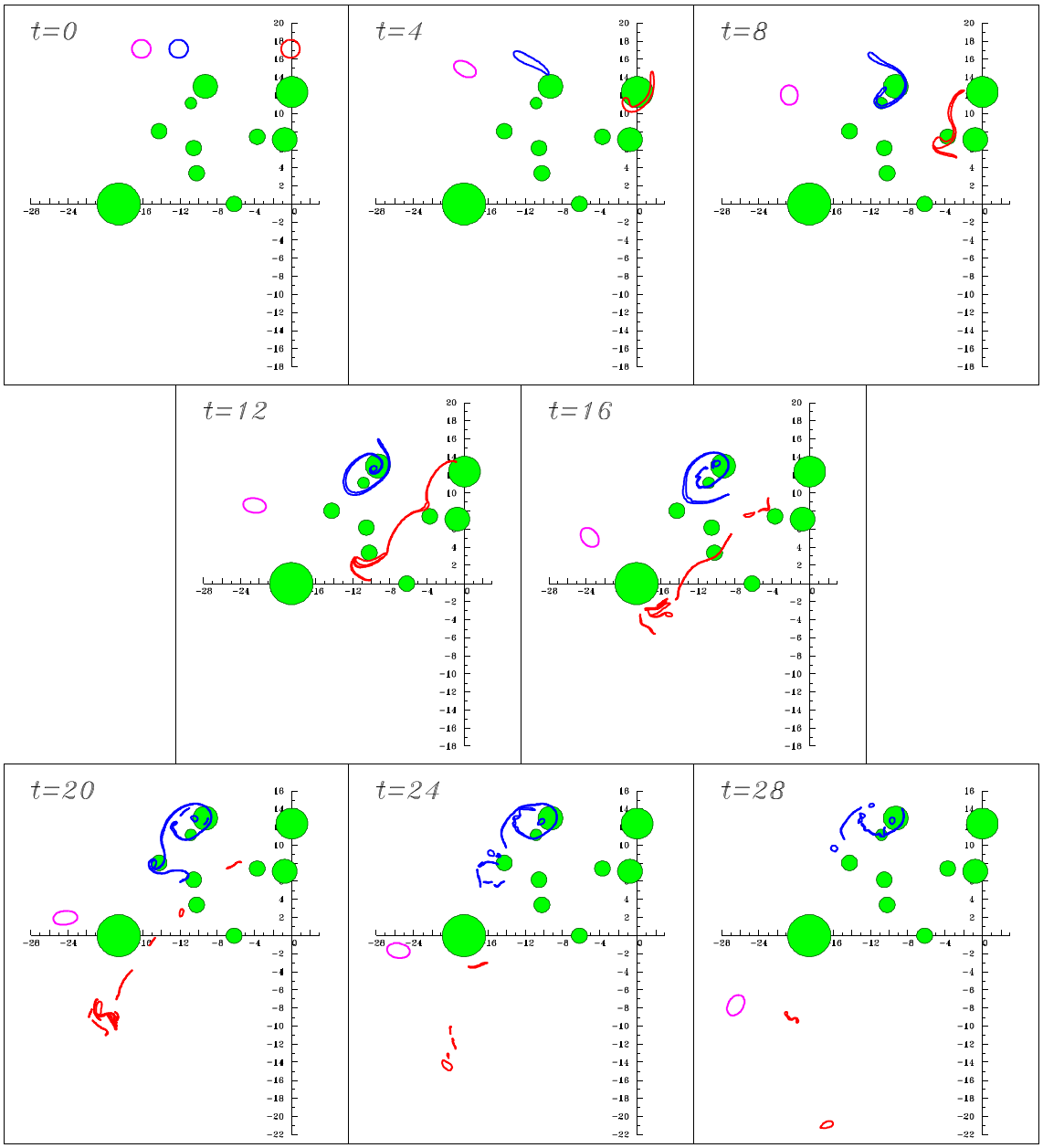

Fig. 14 Motion of initially collinear structures composed of three anticyclonic vortex patches starting from positions **a** (*lilac line*), **c** (*blue line*) and **d** (*red line*) over the submarine ridge

This was observed for both vortex polarities, with the rate of erosion growing from a few percent to about 35–50 % as the vortex radius was reduced from 2 to 1 deformation radius. It must also be noted that small cyclones were not eroded, whereas small anticyclones were completely eroded. This can be related to the difference in motion between these vortices (the cyclones drifting around the seamounts and the anticyclones being drawn towards the seamounts).

4. The detailed initial shape of the vortex did not appear essential for their evolution, if the initial vortex position was close enough to the seamount chain. Consequently, the instability of strongly elongated anticyclonic ellipses did not have time to develop, and these vortices were wrapped around the closest seamount. This wrapping led to a gathering of the vortex volume as it finally escaped the seamount flow. Thus, the regional and topographic flow influence dominated the instability of an isolated vortex.

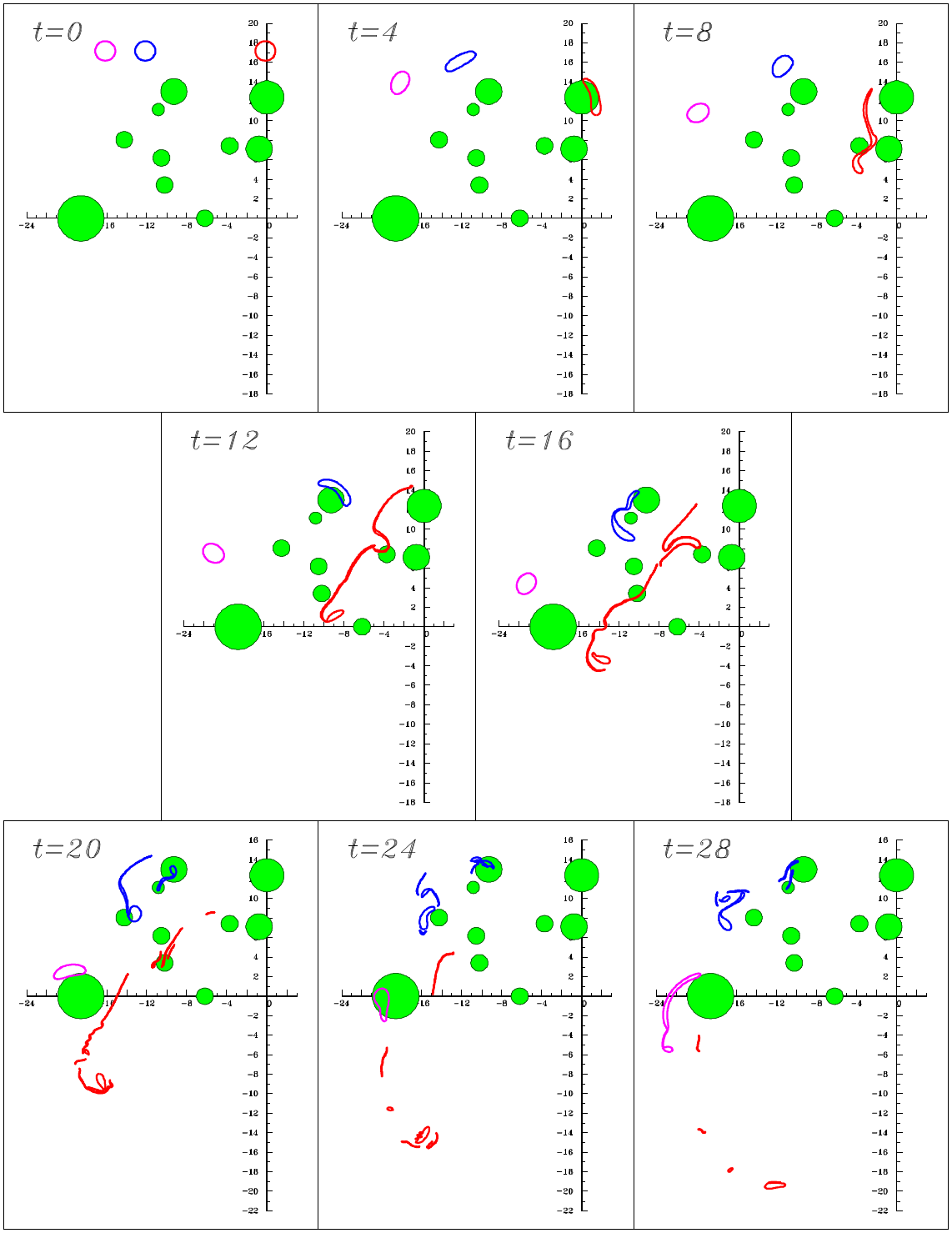

Fig. 15 Same as Fig. 14 but for cyclonic eddies

5. When several vortices were initialized north of the seamount chain, the regional and topographic flow influence were again stronger than that created by the group of vortices. But this latter could weakly modify the vortex trajectories so that they escape erosion and/or trapping by large seamounts. It is of interest to note that many small fragments were produced by that process.

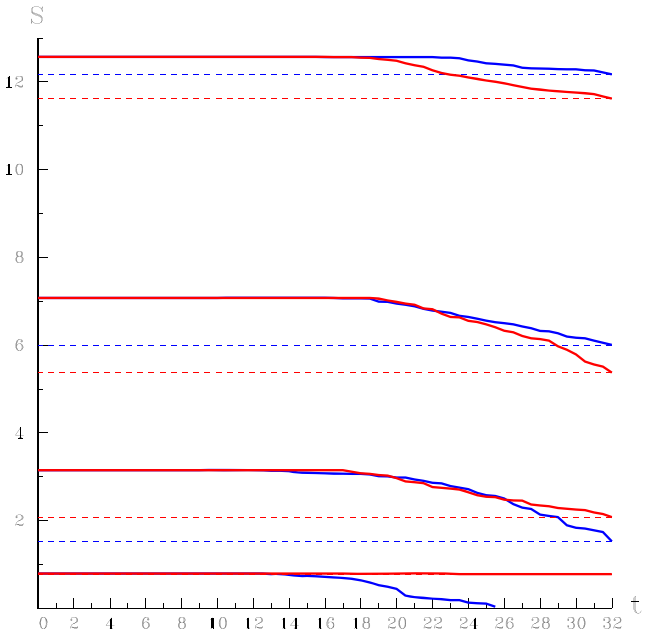

Fig. 16 Time series of the anticyclone (*blue*) and cyclone (*red*) area S for initial radii R=0.5, 1.0, 1.5, 2.0 (eddies initially at point **c**)

In summary, this seamount chain is an efficient obstacle to medium-scale anticyclone propagation and survival, via the action of tall and wide seamounts. In the ocean, observations of meddy interactions at high resolution both spatially and temporally (along with a wide spatial coverage of measurements) have not been achieved yet. The most appropriate technique to obtain a synoptic view of a MW eddy field is their seeding with RAFOS floats (Swallow 1969; Richardson et al. 1989). ARGO profiling floats are also useful to identify MW eddies (Demidov et al. 2012), though these floats have not always been seeded in regions maximizing their chance of collisions with seamounts. CTD recordings can provide fine structure measurements of meddies when they have interacted with topography (Filyushkin et al. 2002; Bashmachnikov et al. 2009), but again it is not possible to predict with accuracy the location of a meddy with only surface data.

Here, we compare qualitatively the trajectories of some meddies tracked with RAFOS floats during the AMUSE experiment, with the results of our model experiments. The eddy trajectory from the westernmost initial position (lilac contours in Fig. 7) can be compared with meddies 4, 6, 9 (Fig. 4). The average meddy drift was cyclonic around the Horseshoe seamounts. Meddies 4 and 6 first moved towards seamount **2** (Fig. 2), then their trajectories separated, but the general motion remained westward. Meddy 4 further approached seamount **7**, and circling seamount **3** moved into the deep ocean. Qualitatively, this corresponds to the eddy motion in the experiments shown in Fig. 7.

The passage of meddies 5 and 11 across the Horseshoe seamount chain between seamounts **1** and **2** up to seamounts **7** and **8** is also interesting. Figure 4 shows that their trajectories stopped (simultaneously with a sharp drop in temperature recording); our simulations (red contours in Figs. 7 and 8) also showed the complete destruction of such eddies into many filaments inside the Horseshoe seamount chain. The decay of meddies 13 and 19 (Fig. 4) near seamounts **5** and **9** has similarities with the situation illustrated in Fig. 9 where a partial capture of the meddy volume by seamount **1** occurred, and the other part of the eddy transformed into filaments. The realism of such a situation is confirmed by observations of meddy interaction with Seine seamount (seamount **10** in Fig. 2), located south of the Horseshoe seamounts; this event was identified during the OASIS experiment (OceAnic Seamounts: an Integrated Study) in 2003–2004 (Bashmachnikov et al. 2009). A close contact of a meddy with the Seine seamount occurred, starting in December 2003. This meddy had a single salinity core at 1100–1200 m depth. Filaments with high salinity were observed in the area adjacent to the seamount. Admittedly, these filaments (or meddy fragments) were captured by the seamount and rotated with a period of about 2 months. Observations seemed to exclude their further merger with the meddy core. After a few rotations around the seamount, the meddy was expelled to the east by the Azores Current after June 2004. Due to this long and close contact, the meddy left the seamount without a part of its core.

Our model experiments are therefore in qualitative agreement with field observations. The escape rate is about 1/3 in the model for anticyclones, and the survival rate for meddies south of the Horseshoe seamount (and into the Canary Basin) is 31 %. The rate of erosion is about 50 % in the model, and the rate of collisions of meddies is about 70 % in observations (though we do not have an estimate for the rate of decay in terms of volume). Qualitatively, meddy volume loss due to topographic interaction was confirmed by the study of the distribution of meddy volume in the Eastern North Atlantic (Fig. 3 in Filyushkin and Sokolovskiy 2011). This study showed that the meddies with the largest volumes drifted to the southwest along the Moroccan coast and to the west of the Horseshoe Seamount chain. Only meddies of small volumes were observed south of this seamount chain.

Naturally, future process studies should include a higher vertical resolution, more realistic topography and vortex shape while still retaining few parameters for sensitivity studies. Such studies will allow a quantitative comparison with regional primitive-equation models when these latter have reached a very high resolution (1×1 km horizontally and 40 m vertically), in particular for the study of filaments and of Mediterranean Water mixing.

Acknowledgments The authors would like to thank Olga Yakovenko for technical assistance and anonymous reviewers for useful remarks. This study was supported by the Russian Foundation for Basic Research

(Projects 13-05-00463, 13-05-00972), RFBR/CNRS (Project 11–05–91052), Ministry of Education of the RF (Project 2.1.1/554). The last author acknowledges the funding of the SEMANE program by SHOM and by IFREMER and current support by CNRS under the PICS program "Geophysical Vortices".

References

Aleynik DL (1998) The structure and evolution of a meddy and Azores frontal zone in autumn 1993. Oceanology 38:312–322

Aleynik DL, Plakhin EA, Filyushkin BN (1998) On the mechanism of formation of intra-thermocline lenses in the canyon area of the Gulf of Cadiz continental slope. Oceanology 38:645–653

Alves JMR, Carton X, Ambar I (2011) Hydrological structure, circulation and water mass transport in the Gulf of Cadiz. Int J Geosci 2:432–456

Ambar I (1983) A shallow core of Mediterranean water off western Portugal. Deep-Sea Res 30:677–680

Ambar I, Serra N, Neves F, Ferreira T (2008) Observations of the Mediterranean Undercurrent and eddies in the Gulf of Cadiz during 2001. J Marine Syst 71:195–220

Armi L, Hebert D, Oakey N, Price JF, Richardson PL, Rossby HT, Ruddick B (1989) Two years in the life of a Mediterranean salt lens. J Phys Oceanogr 19:354–370

Armi L, Zenk W (1984) Large lenses of highly saline Mediterranean water. J Phys Oceanogr 14:1560–1576

Baringer MO, Price JF (1997) Mixing and spreading of the Mediterranean outflow. J Phys Oceanogr 27:1654–1677

Bashmachnikov I, Carton X (2012) Surface signature of Mediterranean water eddies in the Northeastern Atlantic: effect of the upper ocean stratification. Ocean Sci 8:931–943

Bashmachnikov I, Boutov D, Dias J (2013) Manifestation of two meddies in altimetry and sea-surface temperature. Ocean Sci 9:249–259

Bashmachnikov I, Mohn C, Pelegrı JL, Martins A, Jose F, Machı F, White M (2009) Interaction of Mediterranean water eddies with Sedlo and Seine Seamounts, subtropical Northeast Atlantic. Deep-Sea Res II 56:2593–2605

Bower AS, Armi L, Ambar I (1997) Lagrangian observations of meddy formation during A Mediterranean Undercurrent Seeding Experiment. J Phys Oceanogr 27:2545–2575

Carton X, Cherubin L, Paillet J, Morel Y, Serpette A, Le Cann B (2002) Meddy coupling with a deep cyclone in the Gulf of Cadiz. J Marine Syst 32:13–42

Carton X, Daniault N, Alves J, Cherubin L, Ambar I (2010) Meddy dynamics and interaction with neighboring eddies southwest of Portugal: observations and modeling. J Geophys Res 115, C06017. doi:10.1029/2009JC005646

Cherubin L, Carton X, Paillet J, Morel Y, Serpette A (2000) Instability of the Mediterranean water undercurrents southwest of Portugal: effects of baroclinicity and of topography. Oceanol Acta 23:551–573

Daniault N, Maze JP, Arhan M (1994) Circulation and mixing of the Mediterranean Water West of the Iberian Peninsula. Deep-Sea Res 14:1685–1714

Demidov AN, Filyushkin BN, Kozhelupova NG (2012) Detection of Mediterranean lenses in the Atlantic Ocean by profilers of the Argo Project. Oceanology 52:171–180

Diansky NA, Bagno AV, Zalesny VB (2002) Sigma model of global ocean circulation and its sensitivity to variations in wind stress. Izv Atmos Ocean Phys 39:477–494

Dykhno LA, MorozovYG NSV, Filyushkin BN, Shilov IA (1991) Breakup of lenses of Mediterranean water on interaction with bottom relief. Oceanology 31:38–41

Fedorov KN (1978) The thermohaline finestructure of the ocean. Pergamon Press, Oxford Eng and New York, p. 170

Filyushkin BN (1989) Investigation of intrathermocline lenses of Mediterranean origin (Cruise 16 of R/V "Vityaz", June 3–September 16, 1988). Oceanology 29:535–536

Filyushkin BN, Moshonkin SN, Kozhelupova NG (2008) Seasonal evolution of the Mediterranean water propagation in the North Atlantic. Oceanology 48:771–779

Filyushkin BN, Plakhin EA (1996) Experimental study of the first stage of Mediterranean water lens formation. Oceanology 35:797–804

Filyushkin BN, Sokolovskiy MA (2011) Modeling the evolution of intrathermocline lenses in the Atlantic Ocean. J Mar Res 69:191–220

Filyushkin BN, Aleynik DL, Gruzinov VM, Kozhelupova NG (2002) Dynamic degradation of the Mediterranean lenses in the Atlantic Ocean. Dokl Earth Sci 387:1079–1082

Filyushkin BN, Sokolovskiy MA, Kozhelupova NG, Vagina IM (2011a) Reflection of intrathermocline eddies on the ocean surface. Dokl Earth Sci 439(Part 1):986–989

Filyushkin BN, Sokolovskiy MA, Kozhelupova NG, Vagina IM (2011b) Evolution of intrathermocline eddies moving over a submarine hill. Dokl Earth Sci 441(Part 2):1757–1760

Herbette S, Morel Y, Arhan M (2003) Erosion of a surface vortex by a seamount. J Phys Oceanogr 33:1664–1679

Herbette S, Morel Y, Arhan M (2005) Erosion of a surface vortex by a seamount on the beta plane. J Phys Oceanogr 35:2012–2030

Johnson JL, Ambar I, Serra N, Stevens I (2002) Comparative studies of the spreading of Mediterranean water through the Gulf of Cadiz. Deep-Sea Res II 49:4179–4193

Kamenkovich VM, Koshlyakov MN, Monin AS (1986) Synoptic eddies in the ocean. Kamenkovich V.M. (ed). Kluwer Academic Publishers, Dordrecht, p. 444

Käse RH, Zenk W (1987) Reconstructed Mediterranean salt lens trajectories. J Phys Oceanogr 17:158–161

Kozlov VF (1983) Models of topographical vortices in the ocean. Nauka, Moscow, p 200

Le Cann B, Speer K, Serpette A, Paillet J, Reynaud T (1999) Lagrangian observation in the intergyre North-East Atlantic during the ARCANE and EUROFLOAT Projects: early results. Int WOCE Newslett 34:25–27

Madelain F (1970) Influence de la topographie du fond sur l'écoulement Méditerranéen entre le Détroit de Gibralter et le cap Saint-Vincent. Cah Oceanogr 1:43–62, XII annee

Makarov VG (1991) Computational algorithm of the contour dynamics method with changeable topology of domains under study. Model Mech 5(22):83–95 (In Russian)

Morel Y (1995) The influence of an upper thermocline current on intrathermocline eddies. J Phys Oceanogr 267:23–51

Morel Y, McWilliams JC (1997) Evolution of isolated interior vortices in the ocean. J Phys Ocean 27:727–748

Paillet J, Le Cann B, Serpette A, Morel Y, Carton X (1999) Real-time tracking of a northern meddy in 1997–98. Geophys Res Lett 26:1877–1880

Paillet J, Le Cann B, Carton X, Morel Y, Serpette A (2002) Dynamics and evolution of a northern Meddy. J Phys Oceanogr 32:55–79

Peliz A, Dubert J, Marchesiello P, Teles-Machado A (2007) Circulation in the Gulf of Cadiz: model and mean flow structure. J Geophys Res 112, C11015. doi:10.1029/2007JC004159

Prater MD, Sanford TB (1994) A meddy off Cape St. Vincent. Part 1: description. J Phys Oceanogr 24:1572–1586

Richardson PL, Bower AS, Zenk W (1999) Summary of meddies tracked by floats. Int WOCE Newslett 34:18–20

Richardson PL, Tychensky A (1998) Meddy trajectories in the Canary Basin measured during the SEMAPHORE experiment, 1993–1995. J Geophys Res 103:25029–25045

Richardson PL, Walsh D, Armi L, Schr der M, Price JF (1989) Tracking three meddies with SOFAR floats. J Phys Oceanogr 19:371–383

Serra N, Ambar I (2002) Eddy generation in the Mediterranean undercurrent. Deep-Sea Res II 49:4225–4243

Serra N, Sadoux S, Ambar I (2002) Observations and laboratory modeling of meddy generation of Cape St Vincent. J Phys Oceanogr 32:3–25

Shapiro GI, Meschanov SL (1996) Spreading pattern and mesoscale structure of Mediterranean outflow in the Iberian Basin estimated from historical data. J Mar Syst 7:337–348

Shapiro GI, Meschanov SL, Emelianov MV (1995) Mediterranean lens "Irving" after its collision with seamounts. Oceanol Acta 18:309–318

Sokolovskiy MA (1991) Modeling three-layer vortex motions in the ocean by the contour dynamics method. Izv Atmos Ocean Phys 27:550–562

Sokolovskiy MA, Zyryanov VN, Davies PA (1998) On the influence of an isolated submerged obstacle on a barotropic tidal flow. Geophys Astrophys Fluid Dyn 88:1–30

Sparrow M, Boebel O, Zervakis V, Zenk W, Cantos-Figuerola AN, Gould WJ (2002) Two circulation regimes of the Mediterranean outflow revealed by Lagrangian measurements. J Phys Oceanogr 32:1322–1330

Stammer D, Hinrichsen H-H, Käse RH (1991) Can meddies be detected by satellite altimetry? J Gephys Res 96:7005–7014

Sutyrin G, Herbette S, Carton X (2011) Deformation and splitting of baroclinic eddies encountering a tall seamount. Geophys Astrophys Fluid Dyn 105:478–505

Sutyrin GG (2006) Critical effects of a tall seamount on a drifting vortex. J Mar Res 64:297–317

Swallow JG (1969) A deep eddy off Cape St. Vincent. Deep-Sea Res 16:285–295

Tychensky A, Carton X (1998) Hydrological and dynamical characterization of meddies in the Azores region: a paradigm for baroclinic vortex dynamics. J Geophys Res 103:25,061–25,079

Vandermeirsch F, Morel Y, Sutyrin G (2001) The net advective effect of a vertically sheared current on a coherent vortex. J Phys Oceanogr 31:2210–2225

Wang G, Dewar WK (2003) Meddy–seamount interactions: implications for the Mediterranean salt tongue. J Phys Oceanogr 33:2446–2461

Yegorikhin VD, Ivanov YA, Kort VG, Koshlyakov MN, Lukashev YE, Morozov EG, Ovchinnikov IM, Paka VT, Tsybaneva TB, Shadrin IF, Shapovalov SM (1987) An intrathermocline lens of Mediterranean water in the tropical North Atlantic. Oceanology 27:121–127

Zhurbas VM, Kuzmina NP (1981) On mixed patch spread in rotating stably stratified fluid. Izv Atmos Ocean Phys 17:286–295